

Realizing the Haldane phase with bosons in optical lattices

Junjun Xu,^{1,2} Qiang Gu,^{1,*} and Erich J. Mueller^{2,†}

¹*Department of Physics, University of Science and Technology Beijing, Beijing 100083, China*

²*Laboratory of Atomic and Solid State Physics, Cornell University, Ithaca, New York 14853, USA*

(Dated: March 20, 2017)

We analyze an experimentally realizable model of bosons in a zig-zag optical lattice, showing that by rapidly modulating the magnetic field one can tune interaction parameters and realize an analog of the Haldane phase. We explain how quantum gas microscopy can be used to detect this phase's non-local string order and its topological edge states. We model the detection process. We also find that this model supports a supersolid phase, but argue that it only occurs at parameter values which would be challenging to realize in an experiment.

In the past 30 years, one of the dominant themes in condensed matter theory has been the search for models where the collective excitations behave like particles whose properties are unlike any known fundamental particle. While many such fractionalized and topologically ordered models have been found [1], very few of them have been experimentally realized. Here we show how to build on a setup proposed by the NIST cold atom experimental group [2] to explore one of the iconic fractionalized phases, the Haldane phase of a spin-1 chain [3].

In 1983, Haldane showed that the properties of integer and half-integer spin chains can be profoundly different [3, 4]. Over the following decade, several researchers explored the rich properties of the integer spin chain, finding half integer spin edge modes [5–7], and non-local string order [8–10]. More recently, Dalla Torre, Berg, and Altman noted that similar physics should occur for spinless bosons hopping on a one-dimensional lattice: the occupation numbers on each site plays the role of the different spin states [11, 12]. Subsequently, analogs of the Haldane phase have been predicted for a number of one-dimensional Bose-Hubbard models with off-site interactions [13–16]. One enlarges the parameter range over which the Haldane phase is stable if there is a constraint on the maximum number of particles per site. By combining a number of experimental techniques, we show how to realize a model which would be expected to support the Haldane phase. We use Density Matrix Renormalization Group (DMRG) techniques to calculate the properties of this model [17, 18], and explain how to detect the exotic signatures of the Haldane phase.

In a system of 1D lattice bosons, the Haldane (HI) phase lies at the intersection of the density wave (DW) phase, where double occupied sites (doublons) alternate with empty sites (holons), the Mott insulator (MI) phase, where each site is occupied by a single atom, and the superfluid (SF) phase, where the quasiparticles (doublons and holons) are free to move around. In the Haldane phase the quasiparticles are fluid but ordered: their spacing varies, but as one moves from left to right the next quasiparticle after a doublon is a holon, and vice-versa.

This ground state is four-fold degenerate in a large but finite system with hard-wall boundary conditions – corresponding to the flavors of the leftmost and rightmost quasiparticles – which are bound to the edges of the system.

Anisimovas et al. showed that by using a one-dimensional spin dependent optical lattice and Raman induced hopping, one could produce the zig-zag lattice illustrated in Fig. 1(a), described by the tight-binding model [2]

$$H = t_D \sum_j (c_{1,j}^\dagger c_{-1,j} + c_{1,j-1}^\dagger c_{-1,j} + \text{H.c.}) - t \sum_{j,s} (c_{s,j+1}^\dagger c_{s,j} + c_{s,j}^\dagger c_{s,j+1}) + \frac{U_1}{2} \sum_{j,s} n_{s,j} (n_{s,j} - 1) + U_2 \sum_j [n_{1,j} + n_{-1,j-1}] n_{-1,j}. \quad (1)$$

Here $s = \pm 1$ labels the spin state of the atoms and j is the position of the atom along the lattices. t_D and t characterize the hopping between and within these two spin states. U_1 and U_2 describe the on-site and nearest interspecies interaction. Following Anisimovas et al, in the top figure we interpret the spin as a “synthetic dimension.” Physically, the Wannier states of the two spin states lie in a line, alternating one spin-state with another, as illustrated in the bottom figure. We will generally use this latter interpretation, and introduce operators $b_{2j} = c_{-1,j}$ and $b_{2j+1} = c_{+1,j}$, in which case t_D, t are interpreted as nearest and next-nearest neighbor hopping parameters, while U_1, U_2 are on-site and nearest neighbor interaction parameters, i.e. $H = t_D \sum_i (b_{i+1}^\dagger b_i + b_i^\dagger b_{i+1}) - t \sum_i (b_{i+2}^\dagger b_i + b_i^\dagger b_{i+2}) + \frac{U_1}{2} \sum_i n_i (n_i - 1) + U_2 \sum_i n_{i+1} n_i$. Aside from the longer range hopping, Eq. (1) maps onto the model introduced by Dalla Torre et al. in considering polar molecules in optical lattices. Unfortunately, based on their analysis, one expects that the Haldane phase is not stable when U_1/U_2 is large – which is the physically relevant regime considered in [2]. (Our numerics confirm this expectation.) Here we argue that by using a Feshbach resonance, one can reduce U_1 , driving the system into the Haldane phase. The lossy nature of bosonic

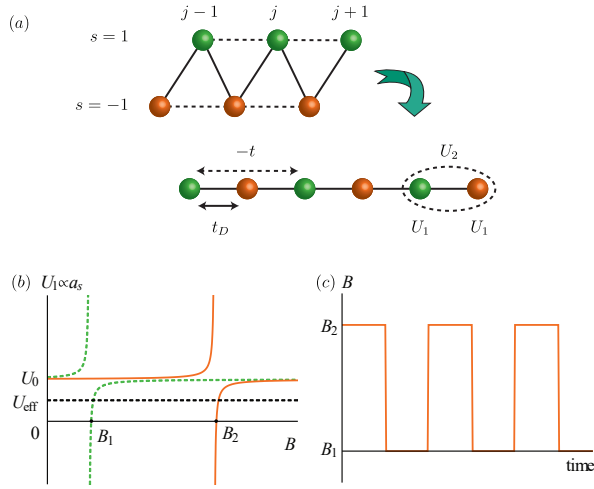


FIG. 1. (a) Schematic of the experimental system, which can be interpreted as a zig-zag ladder or a one-dimensional lattice with next-nearest neighbor hopping. The green and orange colors label two different spin states $s = \pm 1$. (b) On-site interaction U_1 in $F = 1$, $m_F = 0$ (green dashed) and $m_F = 1$ (solid orange) hyperfine states of ^{87}Rb . The background interaction strength U_0 corresponds to the value of U_1 away from the Feshbach resonances near the zero-crossings at B_1 and B_2 . Rapidly switching the magnetic field between B_1 and B_2 , as illustrated in (c), yields an effective time-averaged on-site interaction $U_{\text{eff}} = U_0/2$ in both channels.

Feshbach resonances aids us, as the quantum Zeno effect converts the resulting large 3-body recombination rate into a suppression of the probability of having more than two particles on any given site – further stabilizing the Haldane phase.

More concretely, we consider the $F = 1$, $m_F = 1, 0$ states of ^{87}Rb . The coefficient U_1 is proportional to the scattering length associated with two atoms in the same magnetic sublevel. As illustrated in Fig. 1(b), this scattering length can be manipulated by applying a magnetic field. Near $B_1 \sim 661.43\text{G}$ there is a zero-crossing where the interactions between two $m_F = 0$ atoms vanish, while near $B_2 \sim 685.43\text{G}$ there is a similar zero crossing for $m_F = 1$ [19]. We envision rapidly switching the magnetic field between these two fields, as illustrated in Fig. 1(c). As long as the switching time is short compared to the other scales in the problem ($\hbar/U, \hbar/t \sim \hbar/E_R \approx 0.27\text{ms}$ for laser wavelength $\lambda = 789\text{nm}$) the effective interaction in each spin channel will be given by time-averaging the instantaneous Hamiltonian $U_{\text{eff}} = \int_0^t U(\tau) d\tau$ [20–22]. Even though at any given time the interactions in the two channels will be different, this time averaged interaction is the same for each spin species, and U_1 will be the same on all sites. This technique effectively halves the strength of the on-site interaction as in Fig. 1(b). The coefficient U_2 is largely unaffected. We find that one can achieve a ratio of on-site to nearest neighbor interaction of $U_1/U_2 \approx 1.6$, for a lattice depth of $V_0 = 2E_R$. By

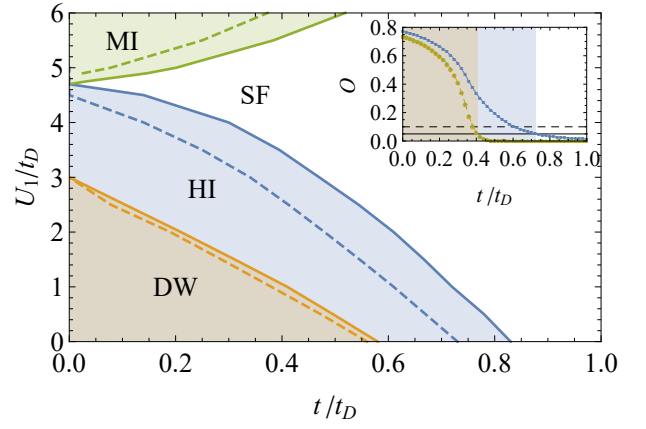


FIG. 2. Phase diagram of the model in Eq. (1), showing regions where experiments observables exceed selected thresholds. Here $U_2/t_D = 2.5$, and the maximum occupation of any site is 2. The solid and dashed boundaries correspond to $O = 0.05/0.1$. Inset shows these order parameters as for $U_1/t_D = 1$ with the solid blue/dotted green/dashed orange lines corresponding to the string/parity/density wave order parameters.

appropriately tuning the transverse confinement, one can take $U_2/t_D = 2.5$, yielding $U_1/t_D = 4$. Figure 2 shows the phase diagram for this model, revealing that these parameters place the system within the Haldane phase regime.

The zero crossings are very close to Feshbach resonances, and hence induce a large 3-body loss rate K_3 . In the present circumstance this is advantageous. Following the logic in [23], when K_3 is large, there is a strong suppression of the process in which a third particle hops onto a site containing two other particles. This suppression can be modelled by a complex on-site three-body repulsion of strength $U_{3b} \sim -i\hbar K_3 n^2/12$. We estimate that one can get $|U_{3b}| \sim 10E_R$ for a typical on-site particle density $n \sim 2.1 \times 10^{15}\text{cm}^{-3}$ and typical on-resonance three-body rate $K_3 \sim 10^{-25}\text{cm}^6/\text{s}$. Since $|U_{3b}|$ is larger than the other scales in the problem, it can be replaced by a constraint that no more than two particles can occupy any site.

With this constraint we use the DMRG to calculate the properties of the model in Eq. (1). This technique is typically understood as systematically optimizing a variational wavefunction in the form of a matrix product state [18]. The degree of approximation is controlled by the bond dimension d . We considered experimentally realizable $L = 60$ sites with one particle per site, and typically take $d = 35$. We systematically varied the bond dimension, and found no significant difference in our results if we further increased d . The algorithm is more efficient if we alter the boundary conditions to break the potential four-fold degeneracy of the Haldane-phase groundstate, and the potential two-fold degeneracy of the density wave groundstate. These boundary conditions pin a vacancy

HI	
SF	
DW	
MI	
SS	

FIG. 3. Typical configurations of occupation numbers extracted from the central 20 sites of our DMRG wavefunctions, modelling single-shot quantum gas microscope images. Configurations correspond to different phases: HI($U_1/t_D = 4$, $U_2/t_D = 2.5$ for $t/t_D = 0$), SF($U_1/t_D = 4$, $U_2/t_D = 2.5$ for $t/t_D = 1$), DW($U_1/t_D = 1$, $U_2/t_D = 2.5$ for $t/t_D = 0$), MI($U_1/t_D = 6$, $U_2/t_D = 2.5$ for $t/t_D = 0$), and SS($U_1/t_D = 0$, $U_2/t_D = 2.5$ for $t/t_D = 0.8$ for maximum occupation number 3). Each circle resembles a single site, and the number in the circle tells how many atoms are on this site. We show two independent realizations for each phase.

at the left-most site, and doublon at the right-most site, but do not alter the physics in the bulk.

The order in the Haldane, Mott insulator, and density wave phases are encoded in string, parity and density wave correlation functions [8, 12]

$$\begin{aligned}
C_{ij}^{\text{str}} &= \left\langle \delta n_i e^{i\pi \sum_{i < k < j} \delta n_k} \delta n_j \right\rangle, \\
C_{ij}^{\text{MI}} &= \left\langle e^{i\pi \sum_{i \leq k \leq j} \delta n_k} \right\rangle, \\
C_{ij}^{\text{DW}} &= (-1)^{j-i} \langle \delta n_i \delta n_j \rangle,
\end{aligned} \tag{2}$$

where $\delta n_k = n_k - 1$. The phase factor $e^{i\pi \sum_{i < k < j} \delta n_k} = \pm 1$ depends on if the number of quasiparticles between sites i and j is even or odd. In the superfluid phase all of the three correlation functions fall to zero as i and j are separated. In the Haldane/Mott insulator phase, only $C^{\text{str}}/C^{\text{MI}}$ is nonzero, while in the density wave phase all the three correlation functions are nonzero.

These correlation functions are directly measurable via a quantum gas microscope [24–28]. One projects the quantum state into one in which there is a definite number of particles on each site – giving a single realization of $\{n_i\}$. Repeating the measurement many times allows one to extract the expectation values in Eq. (2). This technique has already been used to measure the parity order [28].

In addition to using standard techniques to find the expectation values of the various correlation functions, we use a Monte-Carlo sampling algorithm to stochastically

generate ‘typical’ cold-gas microscope images. Given the DMRG wavefunction $|\psi\rangle$, we first calculate the probability that site-1 had 0, 1 or 2 particles on it. We use these probabilities to choose one of these sectors, then project the wavefunction into that sector. This calculation is then repeated on site-2, using the new wavefunction... Figure 3 shows sample configurations generated by this algorithm, which should be representative of what is seen in an experiment. We emphasize that these are not cartoons. As expected, in the HI phase the doublons and holons alternate, with a variable number of singly-occupied sites between them. This can be contrasted with the SF phase, where there is no ordering of the doublons and holons. In the DW phase, doublons and holons alternate. In these images one sees a small number of defects in the order – as should be expected. In the MI phase the images show very few holons and doublons – and those which exist are tightly bound together. In this figure we also show images from a supersolid (SS) phase, which appears when we relax the constraint forbidding double occupancy. This phase, which show density-wave order, but no parity order, is discussed below.

The inset in Fig. 2 shows the different order parameters O , defined as C_{ij} for i, j chosen to be $L/4 = 15$ sites to each side of the center of the chain. In an experiment these would be constructed by averaging over images such as those in Fig. 3, though in our numerics we directly calculate the expectation values from the DMRG wavefunctions. By varying the strength of the Raman beams, one can increase t/t_D . For the parameters in this figure ($U_1/t_D = 1, U_2/t_D = 2.5$), one sees that O^{MI} and O^{DW} rapidly falls to zero at $t/t_D \sim 0.4$, corresponding to a disappearance of the density wave phase. The string order O^{str} , however, persists to much larger values of t/t_D , signalling a Haldane phase. The string order vanishes smoothly, and an experiment will have difficulty pinpointing the exact location of the phase transition: Finite size effects will be significant. The goal of such an experiment, however, is not to precisely identify the phase boundaries – rather it is to produce the exotic Haldane phase. There is clearly a significant range of t/t_D where the parity and density wave order unambiguously vanishes, while the string order is unambiguously finite. Figure 2 shows a “phase diagram,” dividing parameter space into regions which would experimentally be identified through this technique as “MI”, “DW,” “HI,” or “SF.” Finite size scaling would be necessary to identify the true thermodynamic phase boundaries (which are not particularly relevant to the experiment).

The upper row in Fig. 4 shows C_{ij} for i, j chosen to be symmetric to the center of the chain, for parameters corresponding to the density wave, Haldane, and superfluid phase. In all cases one sees that one needs only measure the correlation functions over relatively few sites in order to extract the asymptotic values. The string correlation function appears to reach its asymptotic value quicker

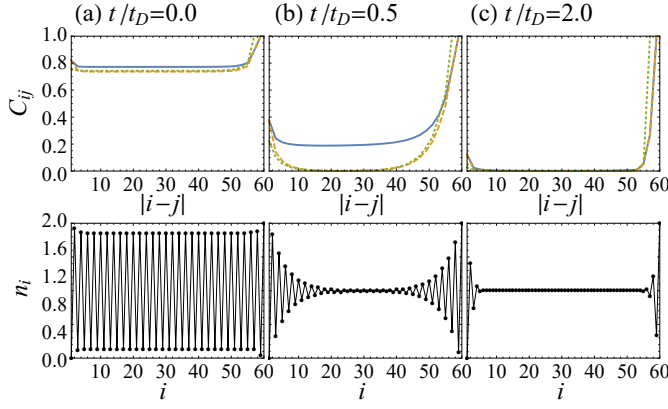


FIG. 4. Local order parameters and particle density in DW/HI/SF phase at $U_1/t_D = 1$, $U_2/t_D = 2.5$ for $t/t_D = 0(a)/0.5(b)/2.0(c)$. The solid blue/dotted green/dashed orange lines label the string/parity/density wave correlation functions.

than the parity and density wave correlation function.

In addition to measuring these correlation functions, one can get information about the various phases by appropriately binning the data, and directly measuring the occupation numbers of the sites. For example, the lower row of Fig. 4 shows the average occupations calculated from images where the left-most site contains a hole, and the right-most site contains a doublon. In the density wave phase, one sees a distinct alternating pattern which extends throughout the chain. In both the Haldane and Superfluid phase this alternating pattern decays as one moves into the bulk, but the decay is much faster in the superfluid phase. One can interpret the structure in the Haldane phase as a signature of the edge modes.

To illustrate the role of the three-body constraint, we repeated our calculations, allowing the on-site particle number to be as large as 3. Figure 5 shows the analog of Fig. 2. The Haldane phase region shrinks and the string order is much harder to discern. Importantly, with the relaxed constraint, one needs a larger value of U_2/U_1 to reach the Haldane phase. In these figures, where $U_2/t_D = 2.5$ is fixed, this feature corresponds to a reduction in the largest value of U_1/t_D at which one finds the Haldane phase. We argue that the smallest easily attainable value of U_1/t_D is 4, suggesting that one will not be able to reach the Haldane phase without the constraint on the particle number, or without using some other technique to increase the strength of nearest-neighbor interactions (see [11] for an approach based on dipolar interactions).

For small on-site interaction U_1 and finite next nearest hopping t , we find a supersolid phase (SS), which displays a non-vanishing density wave order and vanishing parity and Haldane order. This phase is more familiar in the language of the “zig-zag” ladder picture: The atoms form a superfluid which preferentially sits on one leg of the

ladder. An alternative cartoon can be constructed from the DW state “20202020.” Because of the next-nearest neighbor hopping, one can produce a triplon-singlon pair “2020103020,” and these defects may be mobile. Forbidding triple occupancy eliminates these excitations, and is likely responsible for the absence of this phase in the constrained model. In addition to such triplons and singlons, the configurations in Fig. 3 display defects where atoms have hopped from even to odd sublattices. Hence the density wave order is not particularly strong in Fig. 3, and averaging is required to unambiguously identify it.

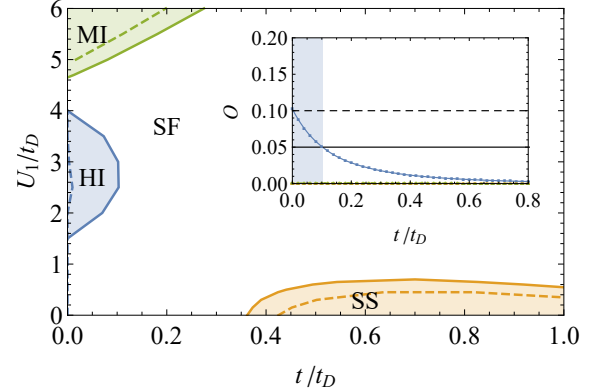


FIG. 5. Phase diagram when maximum occupation of any site is 3. In the inset we choose $U_1/t_D = 3$, and all other parameters and symbols correspond to those in Fig. 2. As illustrated by the inset, the order parameters may be non-zero outside of the shaded regions, but are likely too small to be detected in an experiment.

To summarize, we have proposed a way to realize the Haldane phase in a gas of ^{87}Rb atoms trapped in a zigzag optical lattice, where a different atomic spin state is trapped on each leg of the ladder. One reduces the on-site interactions (relative to the nearest neighbor interactions) by rapidly sweeping the magnetic field between two zero-crossings associated with Feshbach resonances in each of the spin states. The proximity to the Feshbach resonances introduces large three-body loss, which via the quantum Zeno effect prevents triple-occupation. We calculate the phase diagram of this model, and find that the Haldane phase is experimentally realizable. We modelled a quantum-gas microscope experiment, and found that one can readily identify the string order of the Haldane phase in individual images. More quantitative tests require averaging over several images. Such averaging has been used to identify other non-local order parameters [28]. We further show that without the constraint on particle number, this model displays a supersolid phase (cf. [29, 30]). One would need to use other techniques, however, to experimentally reach this supersolid regime. Seeing the string order in the Haldane phase would be a remarkable triumph in engineering quantum matter.

J.X. acknowledges helps from Matthew Reichl on the

numerical calculation. This research is supported by NNSFC (No. 11504021, 11574028), NSF (No. PHY-1508300), CPSF (No. 2015M580043, 2016T90032), and FRFCU (No. FRF-TP-15-040A1).

* qgu@ustb.edu.cn

† em256@cornell.edu

- [1] C. Chiu, J. C. Y. Teo, A. P. Schnyder, and S. Ryu, *Rev. Mod. Phys.* **88**, 035005 (2016).
- [2] E. Anisimovas, M. Račiūnas, C. Sträter, A. Eckardt, I. B. Spielman, and G. Juzeliūnas, *Phys. Rev. A* **94**, 063632 (2016).
- [3] F. D. M. Haldane, *Phys. Lett. A* **93**, 464 (1983); *Phys. Rev. Lett.* **50**, 1153 (1983).
- [4] I. Affleck, *J. Phys.: Condens. Matter* **1**, 3047 (1989).
- [5] I. Affleck, T. Kennedy, E. H. Lieb, and H. Tasaki, *Phys. Rev. Lett.* **59**, 799 (1987); *Commun. Math. Phys.* **115**, 477 (1988).
- [6] M. Hagiwara, K. Katsumata, I. Affleck, B. I. Halperin, and J. P. Renard, *Phys. Rev. Lett.* **65**, 3181 (1990).
- [7] S. H. Glarum, S. Geschwind, K. M. Lee, M. L. Kaplan, and J. Michel, *Phys. Rev. Lett.* **67**, 1614 (1991).
- [8] M. den Nijs and K. Rommelse, *Phys. Rev. B* **40**, 4709 (1989).
- [9] S. M. Girvin and D. Arovas, *Phys. Scr.* **T27**, 156 (1989).
- [10] T. Kennedy and H. Tasaki, *Phys. Rev. B* **45**, 304 (1992); *Commun. Math. Phys.* **147**, 431 (1992).
- [11] E. G. Dalla Torre, E. Berg, and E. Altman, *Phys. Rev. Lett.* **97**, 260401 (2006).
- [12] E. Berg, E. G. Dalla Torre, T. Giamarchi, and E. Altman, *Phys. Rev. B* **77**, 245119 (2008).
- [13] D. Rossini and R. Fazio, *New J. Phys.* **14**, 065012 (2012).
- [14] G. G. Batrouni, R. T. Scalettar, V. G. Rousseau, and B. Grémaud, *Phys. Rev. Lett.* **110**, 265303 (2013).
- [15] S. Ejima, F. Lange, and H. Fehske, *Phys. Rev. Lett.* **113**, 020401 (2014).
- [16] F. Lange, S. Ejima, and H. Fehske, arXiv: 1612.00605.
- [17] S. R. White, *Phys. Rev. Lett.* **69**, 2863 (1992); *Phys. Rev. B* **48**, 10345 (1993).
- [18] U. Schollwöck, *Rev. Mod. Phys.* **77**, 259 (2005); *Ann. Phys.* **326**, 96 (2011).
- [19] A. Marte, T. Volz, J. Schuster, S. Dürr, G. Rempe, E. G. M. van Kempen, and B. J. Verhaar, *Phys. Rev. Lett.* **89**, 283202 (2002).
- [20] S. Blanes, F. Casas, J. A. Oteo, and J. Ros, *Phys. Rep.* **470**, 151 (2009).
- [21] M. Bukov, L. D'Alessio, and A. Polkovnikov, *Adv. Phys.* **64**, 139 (2015).
- [22] A. Eckardt and E. Anisimovas, *New J. Phys.* **17**, 093039 (2015).
- [23] A. J. Daley, J. M. Taylor, S. Diehl, M. Baranov, and P. Zoller, *Phys. Rev. Lett.* **102**, 040402 (2009).
- [24] H. Ott, *Rep. Prog. Phys.* **79**, 054401 (2016).
- [25] W. S. Bakr, J. I. Gillen, A. Peng, S. Fölling, and M. Greiner, *Nature* **462**, 74 (2009).
- [26] W. S. Bakr, A. Peng, M. E. Tai, R. Ma, J. Simon, J. I. Gillen, S. Fölling, L. Pollet, and M. Greiner, *Science* **329**, 547 (2010).
- [27] J. F. Sherson, C. Weitenberg, M. Endres, M. Cheneau, I. Bloch, and S. Kuhr, *Nature* **467**, 68 (2010).
- [28] M. Endres, M. Cheneau, T. Fukuhara, C. Weitenberg, P. Schauß, C. Gross, L. Mazza, M. C. Bañuls, L. Pollet, I. Bloch, and S. Kuhr, *Science* **334**, 200 (2011).
- [29] J. Léonard, A. Morales, P. Zupancic, T. Esslinger, and T. Donner, *Nature* **543**, 87 (2017).
- [30] J. Li, J. Lee, W. Huang, S. Burchesky, B. Shteynas, F. Çagrı Top, A. O. Jamison, and W. Ketterle, *Nature* **543**, 91 (2017).